Environ. Sci. Technol. **1994**, *28*, 1031–1036

Characteristic Times for Limestone Particle Dissolution in the Production of Gypsum from the Wet Flue Gas Desulfurization Process

Amedeo Lancia,[†] Dino Musmarra,[‡] Francesco Pepe,[†] and Gennaro Volpicelli*[,†]

Dipartimento di Ingegneria Chimica, Università "Federico II", P. le V. Tecchio 80, 80125 Napoli, Italy, and Istituto di Ricerche sulla Combustione, C.N.R., P. le V. Tecchio 80, 80125 Napoli, Italy

Limestone dissolution plays a relevant role in determining the quality of the gypsum that can be obtained as a byproduct of the wet limestone flue gas desulfurization process. In this work, the dissolution of limestone in an aqueous solution of SO_2 is experimentally studied. The dissolution rate in a fixed-bed reactor is measured at different sulfur strengths of the solution and liquid–solid relative velocities. The results are interpreted using a model based on the film theory. It is shown that the thickness of the liquid film, and therefore the Sherwood number, is a function of the Reynolds number, and a correlation is proposed for this dependence. Using the correlation and the theoretical model proposed, some results are obtained for the shrinking of a spherical limestone particle as a function of time.

Introduction

The wet limestone flue gas desulfurization (FGD) process is widely used to treat exhaust gases of power plants (*1*, *2*). Such a process has been selected by utility companies because it is the most economical process and is characterized by high SO_2 removal efficiency, low cost, and wide availability of the absorbing reagent and does not require a great knowledge in the management of chemical processes. The difficulties related to the safe disposal of the sludge produced, which is the main disadvantage of this process, could be overcome by obtaining quality gypsum to meet the market specifications. Indeed, although gypsum sale does not pay back the cost of the process, the production of gypsum reduces the problem of solid waste disposal (*3*).

The ability of marketing the byproduct gypsum from FGD processes depends on the supply–demand situation and on the gypsum quality (*4*). The production of gypsum from FGD is very large and continuously growing; therefore, new fields of utilization have to be looked for. Moreover, the properties of FGD gypsum have to be comparable to that of natural gypsum, since stringent specifications on the properties of the gypsum used for building purposes are requested. Important properties of the gypsum include particle size, which determines the slurrying properties; the soluble salts content, even at low level; and the purity, which depends on the absence of impurities in the sorbent used and on the presence of undissolved calcium and magnesium carbonate. In order to obtain high-quality gypsum from flue gas desulfurization, the process must include an efficient particle collection device, a prescrubber loop to remove both hydrogen chloride and fluoride ahead the absorbing tower, and a forced oxidation stage to oxidize the calcium sulfite to sulfate (*3*). Moreover a high-purity limestone is required,

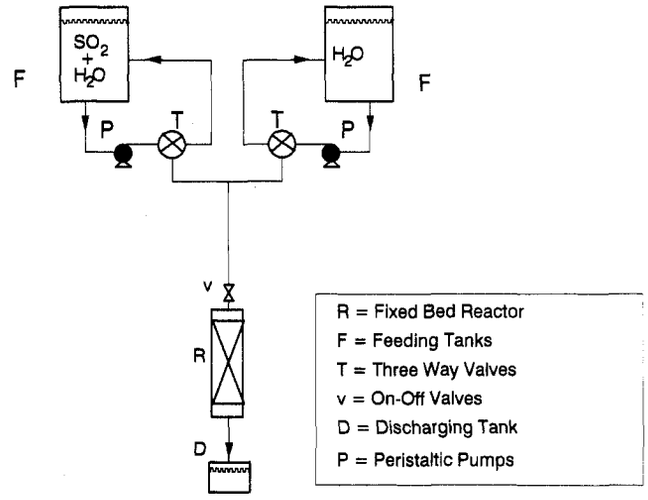

Figure 1. Sketch of the experimental apparatus.

and its dissolution must be carefully controlled to avoid the precipitation of calcium sulfate on the limestone surface, which would give a calcite core in the gypsum particles produced.

Limestone dissolution in acid solutions was mainly studied in connection with the neutralization of acid waters (*5–7*) and with the wet flue gas desulfurization process (*8–10*). The rate of limestone dissolution can be controlled by both the rate of transport of reactants and products between the limestone surface and the bulk solution (*11*) and the rate of heterogeneous reaction at the solid surface (*12–14*); depending upon the hydrodynamic and chemical characteristics of the system, one or both of these steps may limit the dissolution rate. Furthermore, Gage and Rochelle (*15*) showed that high sulfite concentrations can give inhibition effects on the limestone dissolution. A general conclusion (*15*) of the previous studies, for systems with low sulfite concentration and CO_2 partial pressure, is that the dissolution rate of the limestone is diffusion-controlled for acid solution with pH lower than 5.

The object of the present work was to study the limestone dissolution rate in sulfurous solutions with the aim of obtaininig the time characteristic for the complete dissolution of the limestone particles. A model based on the film theory, previously developed by Lancia *et al.* (*16*), has been used to describe the experimental results. The model calculates the mass-transfer rate, the time necessary for complete dissolution of the limestone particles, and the concentration profiles of the dissolved species in the film around the particles. Experimental data for limestone dissolution rate in conditions of controlled liquid–solid relative velocity are reported. A comparison between model and experimental results is analyzed and discussed.

Experimental Section

The experimental apparatus used to measure the amount of dissolved limestone is shown in Figure 1. It

* Author to whom correspondence should be addressed.
† Università "Federico II".
‡ Istituto di Ricerche sulla Combustione.

0013-936X/94/0928-1031$04.50/0

consists of a tubular fixed-bed reactor with feeding and discharging lines. An acrylic reactor 0.016-m i.d. and 0.060-m long was used.

In order to operate with a small reactive surface having a bed high enough to avoid channeling, 1.6 g of limestone particles with sizes in the range of 1–1.4 mm was mixed with inert glass beads, the size of which was close to that of the limestone. A layer of the same inert glass beads preceded the reactant bed so that good liquid distribution was obtained. To ensure reproducible results, the limestone particles were pretreated to remove the adhering calcite dust by washing them with distilled water until the filtrate was clear.

The inlet liquid stream, obtained by acidifying distilled water with reagent-grade H_2SO_3, was fed to the reactor from the reservoir tank by means of a peristaltic pump. A previous calibration of the pump gives the correct flow rate. The temperature of the solution was kept constant in all runs at the value of 25 ± 1 °C. Iodometric titration was employed to measure the total sulfur species concentration in the liquid stream. Such concentration ranged from 500 to 2240 mg/L, expressed as SO_2, giving a pH in the range of 2–3. The calcium concentration in the exit stream was measured by EDTA titration in samples taken in the outlet liquid stream at different times. Different superficial velocities (v) of the liquid ranging between 5.5 and 28.0 cm/s were employed varying the liquid flow rate (L) between 40 and 200 L/h.

Model Equations

The diffusive model set up by Lancia *et al.* (*16*) was used to describe the $CaCO_3$ dissolution in aqueous solutions of SO_2. Such a model is based on the theory proposed by Mullin (*17*), which assumes that two elementary steps in series occur during the dissolution process, *i.e.*, surface reaction and diffusional transport of reactants and products. The first takes place in a very thin surface layer adhering to the particle surface, while the second takes place in the mass-transfer boundary layer. The model by Lancia *et al.* (*16*), on the basis of previous work (*7*), assumes that the diffusion of ions and molecules in the mass-transfer boundary layer is the limiting step of the dissolution process and that thermodynamic equilibrium exists between the species involved.

Limestone dissolution requires the removal of Ca^{2+} and CO_3^{2-} ions from the solid surface. The reaction of CO_3^{2-} ions with the H^+ ions, produced by the dissociation of H_2SO_3 and HSO_3^-, allows the Ca^{2+} surface concentration to increase. As a consequence, the limestone dissolution takes place due to the transport of the species which are originally present at the surface and of those which are produced by the following proton-exchange reactions:

$$H_2SO_3 = H^+ + HSO_3^- \qquad K = 1.39 \times 10^{-2}\ \text{M} \quad (1)$$

$$HSO_3^- = H^+ + SO_3^{2-} \qquad K = 6.70 \times 10^{-8}\ \text{M} \quad (2)$$

$$H_2CO_3 = H^+ + HCO_3^- \qquad K = 4.25 \times 10^{-7}\ \text{M} \quad (3)$$

$$HCO_3^- = H^+ + CO_3^{2-} \qquad K = 4.57 \times 10^{-11}\ \text{M} \quad (4)$$

$$H_2O = H^+ + OH^- \qquad K = 1.00 \times 10^{-14}\ \text{M}^2 \quad (5)$$

where K is the thermodynamic equilibrium constant at 25 °C. Values of K for reactions 1 and 2 are taken from those reported by Goldberg and Parker (*18*), while for reactions 3–5 they are evaluated from data reported by Brewer (*19*).

Table 1. Diffusivity Coefficients for Species Considered in Model Equations

species (ref)	$D \times 10^5$, cm²/s	species (ref)	$D \times 10^5$, cm²/s
H_2CO_3 (*10*)	2.00	H_2SO_3 (*31*)	1.76
HCO_3^- (*10*)	1.20	HSO_3^- (*10*)	1.33
CO_3^{2-} (*10*)	0.70	SO_3^{2-} (*10*)	0.77
Ca^{2+} (*10*)	0.79	OH^- (*10*)	5.27
H^+ (*10*)	9.30		

The phenomena of mass transfer and accompanying instantaneous chemical reactions described above were modeled using the film theory. The equations taken into account are the total material balances (*20*) for calcium, carbon, and sulfur:

$$\frac{dN_{Ca^{2+}}}{dx} = 0 \quad (6)$$

$$\frac{dN_{CO_3^{2-}}}{dx} + \frac{dN_{HCO_3^-}}{dx} + \frac{dN_{H_2CO_3}}{dx} = 0 \quad (7)$$

$$\frac{dN_{SO_3^{2-}}}{dx} + \frac{dN_{HSO_3^-}}{dx} + \frac{dN_{H_2SO_3}}{dx} = 0 \quad (8)$$

where N_I is the molar flux of the I species and x is the normal coordinate in a system having its origin on the boundary between the surface layer and the mass-transfer boundary layer. According to Onsager and Fuoss (*21*) N_I is given by:

$$N_I = -D_I\frac{dc_I}{dx} - F\frac{D_I}{RT}z_I c_I\frac{d\Phi}{dx} \quad (9)$$

where I refers to the species Ca^{2+}, H^+, H_2SO_3, HSO_3^-, SO_3^{2-}, H_2CO_3, HCO_3^-, CO_3^{2-}, and OH^-. In this equation, c_I and z_I are the concentration and the number of the elementary charge of the I species, respectively; D_I is the diffusivity of the I species, the values of which are reported in Table 1; F is the Faraday constant; R is the gas constant; T is the absolute temperature; and $d\Phi/dx$ is the gradient of electric potential. It is worth noting that in transport processes involving charged species, even if there is no applied potential, the condition that there is no net current expressed as:

$$\sum_I z_I N_I = 0 \quad (10)$$

gives for the gradient of electric potential the following equation:

$$\frac{d\Phi}{dx} = -\frac{\sum_I z_I D_I \frac{dc_I}{dx}}{F\sum_I z_I^2 \frac{D_I}{RT}c_I} \quad (11)$$

from which it is obtained that the gradient of electric potential is not zero since the diffusivities are not all equal among them.

Equations 6–8 were solved subject to conditions that the equilibria of reactions 1–5 (see Appendix) together with the electroneutrality equation:

$$\sum_I c_I z_I = 0 \quad (12)$$

had to be respected for every x.

The boundary conditions for the system of eqs 6–8 at $x = 0$ are the following three:

$$N_{Ca^{2+}} = N_{H_2CO_3} + N_{HCO_3^-} + N_{CO_3^{2-}} \quad (13)$$

$$N_{H_2SO_3} + N_{HSO_3^-} + N_{SO_3^{2-}} = 0 \quad (14)$$

and the equilibrium of the reaction

$$CaCO_3 = Ca^{2+} + CO_3^{2-} \qquad K = 4.8 \times 10^{-9}\ M^2 \quad (15)$$

where the value of K is reported by Meites (22).

Such conditions impose the stoichiometric restriction that the rate of calcium ion generation is equal to that of carbon species (eq 13), the absence of net transport of sulfur between the solid and the liquid (eq 14), and the equilibrium of $CaCO_3$ dissolution reaction (eq 15).

On the other hand, at the bulk side ($x = \delta$, where δ is the film thickness), the boundary conditions are

$$c_{Ca^{2+}/x=\delta} = c_{Ca^{2+}/b} \quad (16)$$

$$c_{H_2CO_3/x=\delta} + c_{HCO_3^-/x=\delta} + c_{CO_3^{2-}/x=\delta} = c_{C/b} \quad (17)$$

$$c_{H_2SO_3/x=\delta} + c_{HSO_3^-/x=\delta} + c_{SO_3^{2-}/x=\delta} = c_{S/b} \quad (18)$$

where $c_{I/x=\delta}$ is the molar concentration of I species at $x = \delta$ and $c_{Ca^{2+}/b}$, $c_{C/b}$, $c_{S/b}$ are the sums of the concentrations in the liquid bulk of the species containing calcium, carbon, and sulfur, respectively. The equations described allow us to evaluate the calcium flux ($N_{Ca^{2+}}$) once the liquid bulk composition is known, and a value for δ is assigned.

On the other hand, values of δ can be obtained by integrating the model equations once the calcium flux is experimentally determined. With such purpose, some experimental runs were carried out in the fixed bed reactor varying the liquid–solid relative velocity and the SO_2 concentration in the inlet stream and measuring the Ca^{2+} outlet concentration. The knowledge of the outlet calcium concentration allows the integration of the model equations. Indeed, even if the liquid bulk concentrations and the fluxes change along the bed length l, they can be calculated by integrating the following equation:

$$N_{Ca^{2+}/l}\, dS = L dc_{Ca^{2+}/b} \quad (19)$$

where

$$dS = \frac{S}{l^*}\, dl \quad (20)$$

In these equations $N_{Ca^{2+}/l}$ is the calcium flux at length l along the reactor, S is the limestone surface in contact with the liquid, l^* is the total length of the reactor, and S/l^* gives the limestone surface per unit length of the reactor, which is assumed constant.

The integration of eq 19 with the boundary condition:

$$c_{Ca^{2+}} = c_{Ca^{2+}/in} \quad \text{at} \quad l = 0 \quad (21)$$

gives

$$\frac{S}{l^*}\int_0^{l^*} N_{Ca^{2+}}\, dl = L(c_{Ca^{2+}/out} - c_{Ca^{2+}/in}) \quad (22)$$

where $c_{Ca^{2+}/in}$ and $c_{Ca^{2+}/out}$ are the Ca^{2+} concentration in the inlet and the outlet streams to the reactor, respectively. Equations 19 and 22 state that the increase of calcium concentration along the reactor is due to limestone dissolution.

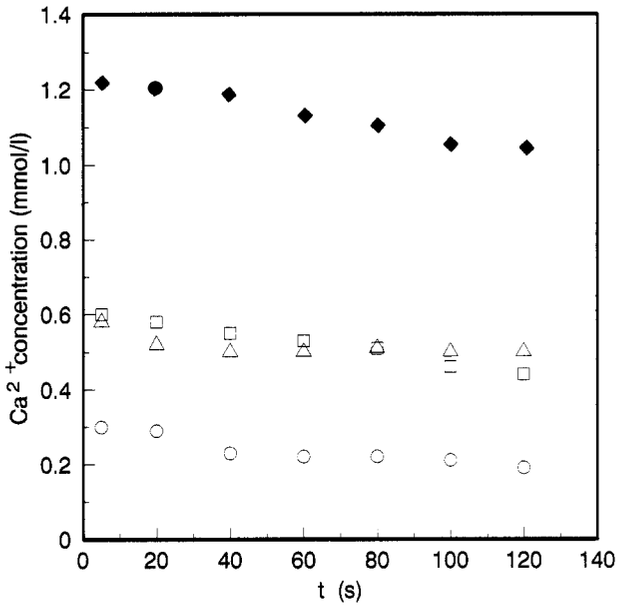

Figure 2. Concentration of Ca^{2+} ions versus time for different SO_2 concentrations and liquid flow rate.

The value of $N_{Ca^{2+}}$ along the bed, which depends on the film thickness, can be evaluated by integrating the model equations 1–18. According to the physical meaning of δ, the integration of the equations was carried out imposing that δ is constant along the bed. The equations were integrated at a finite difference starting the integration at $l = 0$, where the bulk concentrations are known. By means of eq 19, the calcium concentration at $l = l + \Delta l$ can be calculated, while the remaining bulk concentrations at any $l + \Delta l$ are calculated using the equilibrium equation of reactions 1–5, the neutrality equation 12, and the following balance equations:

$$(c_{H_2CO_3} + c_{HCO_3^-} + c_{CO_3^{2-}})_{l+\Delta l} - (c_{H_2CO_3} + c_{HCO_3^-} + c_{CO_3^{2-}})_l = (c_{Ca^{2+}})_{l+\Delta l} - (c_{Ca^{2+}})_l \quad (23)$$

$$(c_{H_2SO_3} + c_{HSO_3^-} + c_{SO_3^{2-}})_{l+\Delta l} - (c_{H_2SO_3} + c_{HSO_3^-} + c_{SO_3^{2-}})_l = 0 \quad (24)$$

Equation 23 is based on the stoichiometry of the limestone dissolution reaction, while eq 24 reflects the conservation of sulfur species in the limestone dissolution process. The value of δ that verifies eq 22 is the right value of the film thickness.

Results and Discussion

The experimental results for some typical experimental runs are shown in Figure 2, in which the measured concentration of dissolved calcium is reported as a function of the run time. This figure shows that a greater SO_2 concentration in the inlet liquid stream and a greater liquid flow rate lead to an increase in the total concentration of

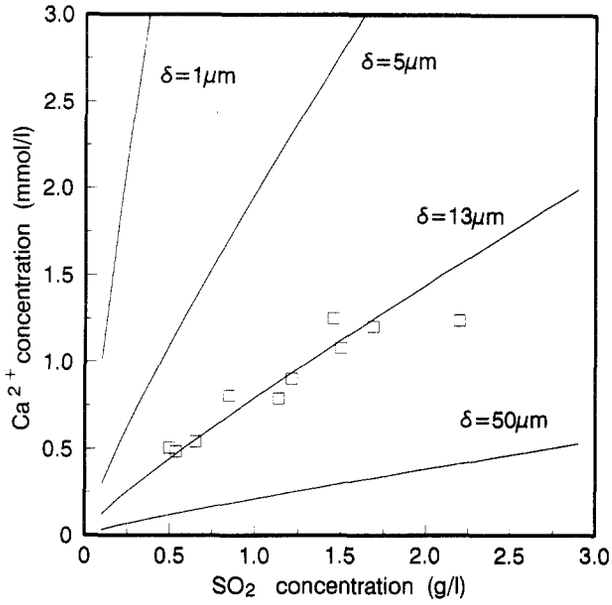

Figure 3. Comparison between Ca^{2+} ions concentration at $t = 0$ as experimentally detected (□) and as calculated by means of the model (—) for different values of the film thickness. L = 44 L/h.

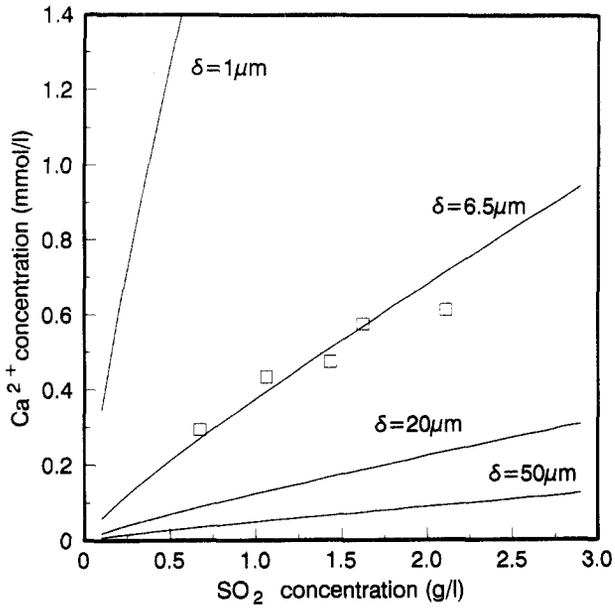

Figure 4. Comparison between Ca^{2+} ions concentration at $t = 0$ as experimentally detected (□) and as calculated by means of the model (—) for different values of the film thickness. L = 190 L/h.

dissolved calcium. Since the system works under unsteady-state conditions, due to nonuniform limestone consumption along the reactor, the results for each run were extrapolated at $t = 0$ to refer to a condition in which the total limestone surface can be evaluated assuming that the limestone particles are equally sized spheres with a diameter of 1.2 mm.

The total concentrations of dissolved calcium, evaluated at $t = 0$, are reported in Figures 3 and 4 versus SO_2 concentration for the experimental runs conducted at L = 44 and L = 190 L/h, which are respectively the smallest and the largest flow rate among those considered. In these figures, the lines represent the results of the model calculations for different values of δ. The values of δ for which the model calculations fit the experimental results are 13 and 6 μm, in conjunction with the liquid flow rates of 44 and 190 L/h.

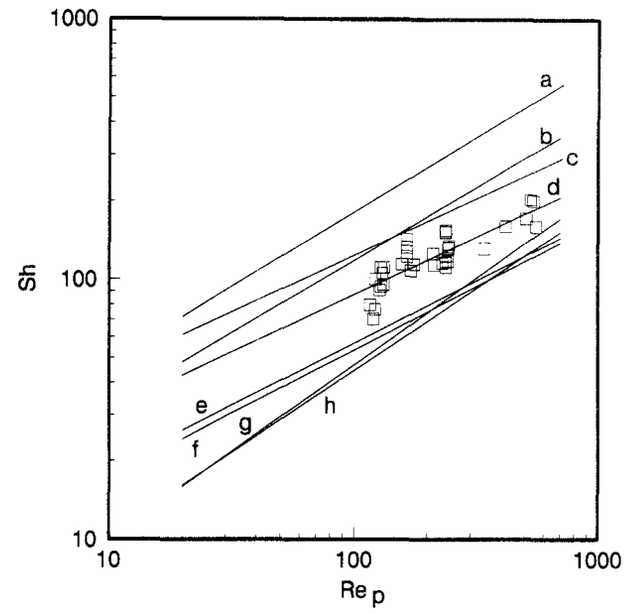

Figure 5. Sherwood number versus particle Reynolds number. Experimental results (□): (a) Gaffney and Drew (*28*), (b) Chu *et al.* (*25*), (c) Hobson and Thodos (*27*), (d) eq 25, (e) Clift *et al.* (*24*), (f) Ranz and Marshall (*23*), (g) Calderbank and Moo-Young (*29*), and (h) Kato *et al.* (*26*).

Model and experimental results reported in Figures 3 and 4 indicate that in the range of superficial velocities of the liquid considered there is a nearly linear relationship between the SO_2 concentration and the total concentration of dissolved calcium. Figures 3 and 4 also show that the value of δ does not depend on SO_2 concentration in the liquid. Such consideration is a good test of the model, which embodied the assumption that the film thickness depends on the physical properties of the fluid, on the particle diameter, and on the liquid–solid relative velocity but is independent of the liquid composition.

The values of δ obtained by means of the model were made dimensionless with respect to particle diameter d_p by means of a Sherwood number (Sh). In the logarithmic plot of Figure 5, the Sherwood number is reported versus the modified particle Reynolds number [$Re_p = \rho v\, d_p/\mu(1 - \epsilon)$, where ρ is the liquid density, μ is the liquid viscosity, and ϵ is the bed voidage fraction]. Such a figure shows that the experimental findings follow a nearly linear dependence. The equation that best fits the experimental results is

$$Sh = 2 + 10.72 Re_p^{0.45} \qquad (25)$$

Figure 5 also reports the more relevant empirical correlations found in the literature for the mass transfer in the film. They include the correlations obtained for the evaporation of liquid drops in the airstream by Ranz and Marshall (*23*) and by Clift *et al.* (*24*); the correlations describing the gas–solid mass transfer in fixed beds of granular solids proposed by Chu *et al.* (*25*) and by Kato *et al.* (*26*); and those proposed by Hobson and Todos (*27*), by Gaffney and Drew (*28*), and by Calderbank and Moo-Young (*29*) for solid dissolution. In Figure 5, such correlations are reported for the Schmidt number, Sc = 633, which is the value calculated considering the diffusivity of Ca^{2+} in water and the density and viscosity of the water at 25 °C. The comparison reported in Figure 5 between experimental results and those obtained from

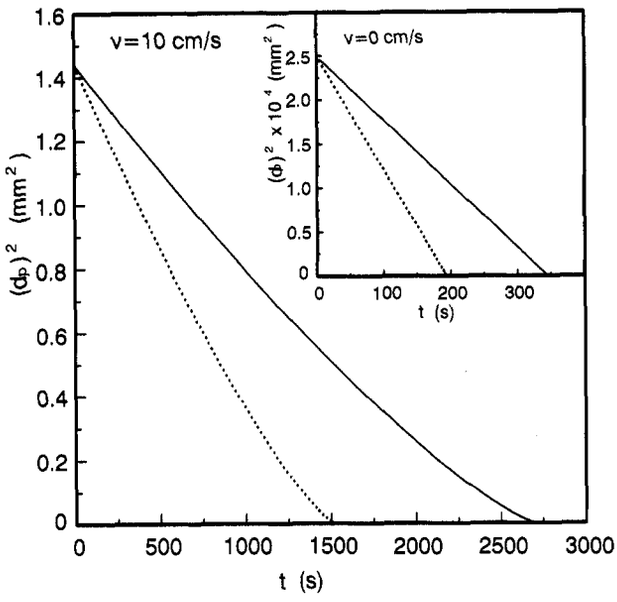

Figure 6. Model calculations of the limestone particle dissolution reported as $(d_p)^2$ versus time. SO_2 concentration in the liquid stream: (···) 1000 mg/L; (—) 500 mg/L.

the previous correlations shows that, in the interval of the Reynolds number tested, the correlations proposed in refs 23, 24, and 27 describe well the mass transfer in the limestone dissolution process.

In order to evaluate the time, t_D, required to complete the dissolution of a single limestone particle, eq 25 together with model equations 1–24 has been employed. Indeed, the value of t_D can be evaluated by the following calcium material balance on a single limestone particle:

$$t_D = \int_{d_p^0}^{0} \frac{\rho_{ms} d(d_p)}{2N_{Ca^{2+}}} \tag{26}$$

Equation 26 requires the dependence between the calcium flux $N_{Ca^{2+}}$ and the particle diameter d_p. The model gives $N_{Ca^{2+}}$ as a function of the film thickness, while eq 25 gives the relationship between δ and d_p for assigned liquid–solid relative velocity.

The shrinking rate of the limestone particle ($d_p^0 = 1200$ μm) calculated by means of eq 26 is reported in Figure 6 as $(d_p)^2$ versus t for two different values of SO_2 concentration in the inlet liquid stream and for a superficial liquid velocity of 10 cm/s. As expected, a greater SO_2 concentration leads to a faster consumption of limestone particle. Furthermore, in order to compare the dissolution rate obtained by the model with those realized in full-scale scrubber systems, in the upper-right corner of Figure 6 values of t_D calculated in conditions ($v = 0$ and $d_p^0 = 50$ μm) closer to those occurring in the scrubbers are reported. In such cases, a linear dependence between $(d_p)^2$ and t was found and a limestone dissolution rate of 2.25×10^{-7} mol/cm^2 s is obtained for the SO_2 inlet concentration of 500 mg/L and for $d_p = 20$ μm. This result is in fair agreement with the rate of limestone dissolution typical of FGD systems (*10*).

Conclusions

The complete dissolution of the limestone particles used as sorbent in flue gas desulfurization processes is required to avoid the presence of impurity in the gypsum to allow its commercialization. The model used in the present work describes well the experimental results of limestone dissolution in sulfurous solutions, showing that in these conditions the process is controlled by diffusive phenomena. Furthermore, it is shown that the thickness of the mass-transfer boundary layer can be evaluated by means of a correlation between the Sherwood number and the Reynolds number and that such a correlation is in agreement with others found in the literature. Characteristic times for limestone particle dissolution have been evaluated, for different operating conditions, applying the proposed model.

Acknowledgments

The authors gratefully acknowledge the useful discussions with Prof. Gary T. Rochelle of the Department of Chemical Engineering of the University of Texas at Austin.

Appendix

The chemical reactions taken into account by the model can be written in the following general form:

$$\sum_I \nu_I I = 0 \tag{A1}$$

where ν_I is the stoichiometric coefficient of the I species and is assumed positive for the reactants and negative for the products. The equilibrium conditions for the reaction (A1) is

$$K = \prod_I a_I^{-\nu_I} \tag{A2}$$

where a_I is the activity of the I of the species.

The activity a_I is related to the molar concentration by

$$a_I = \gamma_I c_I \tag{A3}$$

where γ_I is the activity coefficient.

Values of the activity coefficients can be calculated using an approximate equation derived from the general Debye–Huckel equation as proposed by Harned and Owen (*30*):

$$\ln \gamma_I = -G z_I^2 \frac{\sqrt{E}}{1 + d_I B \sqrt{E}} \tag{A4}$$

where E is the ionic strength of the solution given by

$$E = \frac{1}{2} \sum_I z_I^2 c_I \tag{A5}$$

and G and B are the Debye and Huckel constants, that for aqueous solutions at 25 °C are $G = 1.777$ L$^{1/2}$ mol$^{-1/2}$ and $B = 0.3281 \times 10^8$ L$^{1/2}$ cm^{-1} mol$^{-1/2}$. Since the effective diameters of ions in solution (d_I) are in the range of 3–5 $\times 10^{-7}$ cm, the product Bd_I is approximately equal to unity. Therefore, eq A4 can be written as follows:

$$\ln \gamma_I = -G z_I^2 \frac{\sqrt{E}}{1 + \sqrt{E}} \tag{A6}$$

Notations

a	activity, mol/L
B	Debye–Huckel constant, L$^{1/2}$ cm^{-1} mol$^{-1/2}$
c	concentration, mol/L
D	diffusivity, cm^2/s
d	effective ion diameter, cm

d_p^0	initial particle diameter, mm
d_p	particle diameter, mm
E	ionic strength, mol/L
F	Faraday constant, s A/mol
G	Debye–Huckel constant, $L^{1/2}$ $mol^{-1/2}$
K	thermodynamic equilibrium constant
L	liquid flow rate, L/h
l	reactor axial coordinate, cm
l^*	reactor height, cm
M	molarity, mol/L
N	flux of the species, mol/cm^2 s
R	gas constant, J/mol K
Re_p	particle Reynolds number, dimensionless
S	surface, cm^2
Sc	Schmidt number, dimensionless
Sh	Sherwood number, dimensionless
T	absolute temperature, K
t	time, s
t_D	dissolution time, s
v	superficial velocity of the liquid, cm/s
x	normal coordinate in the film, cm
z	ionic charge, dimensionless

Greek Symbols

γ	activity coefficient, dimensionless
δ	film thickness, mm
ϵ	bed voidage, dimensionless
μ	viscosity, g/cm s
ν	stoichiometric coefficient, dimensionless
ρ	liquid density, g/cm^3
ρ_{ms}	solid molar density, mol/cm^3
Φ	electric potential, J/cm s A

Subscripts

b	liquid bulk
C	total carbon species
I	species: Ca^{2+}, H^+, H_2SO_3,HSO_3^-, SO_3^{2-}, H_2CO_3, HCO_3^-, CO_3^{2-}, OH^-
in	inlet
out	outlet
S	total sulfur species
$x=\delta$	boundary of the liquid film

Literature Cited

(1) Kyte, W. S. *Trans. Inst. Chem. Eng.* **1981**, *59*, 219.
(2) Astarita, G.; Sawage, D. W.; Bisio, A. *Gas Treating with Chemical Solvents*; Wiley Interscience: New York, 1983.
(3) Rosenberg, H. S. *Ind. Eng. Prod. Res. Dev.* **1986**, 25, 348.
(4) Mields, A. *Int. Cement Rev.* **1990**, *11*, 18.
(5) Santoro, L.; Ciambelli, P.; Volpicelli, G. *Chim. Ind.* **1973**, *55*, 577.
(6) Barton, T.; Vatanatham, T. *Environ. Sci. Technol.* **1976**, *10*, 262.
(7) Volpicelli, G.; Caprio, V.; Santoro, L.; Ciambelli, P. *Chem. Eng. J.* **1981**, *21*, 29.
(8) Chan, P. K.; Rochelle, G. T. in *Flue Gas Desulfurization*; Hudson, J. I., Rochelle, G. T., Eds.; ACS Symposium Series 188; American Chemical Society: Washington, DC, 1982; pp 75–97.
(9) Toprac, A. J.; Rochelle, G. T. *Environ. Prog.* **1982**, *1*, 52.
(10) Rochelle, G. T.; Chan, P. K. R.; Toprac, A. T. *Limestone Dissolution in Flue Gas Desulphurization Process*; U.S. EPA: Washington, DC, 1983; EPA-6/7-83-043.
(11) Wallin, M.; Bjerle, I. *Chem. Eng. Sci.* **1989**, *44*, 61.
(12) Terjesen, S. G.; Erga, O.; Thorsen, G.; Ve, A. *Chem. Eng. Sci.* **1961**, *14*, 1977.
(13) Plummer, L. N.; Wigley, T. M. L. *Geochim. Cosmochim. Acta* **1976**, *40*, 191.
(14) Plummer, L. N.; Parkhurst, D. L.; Wigley, T. M. L. in *Chemical Modeling in Aqueous Systems*; Jenne, E. A., Ed.; ACS Symposium Series 93; American Chemical Society: Washington, DC, 1979; pp 537–573.
(15) Gage, C. L.; Rochelle G. T. *J. Air Waste Manage. Assoc.* **1992**, *42*, 926.
(16) Lancia, A.; Musmarra, D.; Pepe, F.; Volpicelli, G. *Chem. Eng. Sci.* **1991**, *46*, 2507.
(17) Mullin, J. W. *Crystallization*, 3rd ed.; Butterworths-Heineman: London, 1993; p 215.
(18) Goldberg, R. N.; Parker V. B. *J. Res. Natl. Bur. Stand. (U.S.)* **1985**, *90*, 314.
(19) Brewer, L. in *Flue Gas Desulfurization*; Hudson, J. I., Rochelle, G. T., Eds.; ACS Symposium Series 188; American Chemical Society: Washington, DC, 1982; pp 1–39.
(20) Olander, D. R. *AIChE J.* **1960**, *6*, 233.
(21) Onsager, R.; Fuoss R. M. *J. Phys. Chem.* **1932**, *36*, 2689.
(22) Meites, L., Ed. *Handbook of Analytical Chemistry*; McGraw-Hill: New York, 1963; pp 1–13.
(23) Ranz, W. E.; Marshall, W. R., Jr. *Chem. Eng. Prog.* **1954**, *48*, 141.
(24) Clift, R.; Grace, J. R.; Weber, M. E. *Bubbles, Drops and Particles*; Academic Press: New York, 1978.
(25) Chu, J. C.; Kalil, J.; Wetteroth, W. A. *Chem. Eng. Prog.* **1953**, *48*, 141.
(26) Kato, K.; Kubota, H.; Wen, C. Y. *Chem. Eng. Prog. Symp. Ser.* **1970**, *66*, 87.
(27) Hobson, M.; Thodos, G. *Chem. Eng. Prog.* **1949**, *45*, 517.
(28) Gaffney, B. J.; Drew, T. B. *Ind. Eng. Chem.* **1950**, *42*, 1120.
(29) Calderbank, P. H.; Moo-Young, M. B. *Chem. Eng. Sci.* **1961**, *16*, 39.
(30) Harned, H. S.; Owen, B. B. *The Physical Chemistry of Electrolitic Solution*; Reinhold: New York, 1958.
(31) Pasiuk-Bronikowska, W.; Rudzinski, K. J. *Chem. Eng. Sci.* **1991**, *46*, 2281.

Received for review June 1, 1993. Revised manuscript received December 7, 1993. Accepted February 17, 1994.[⊗]

[⊗] Abstract published in *Advance ACS Abstracts,* April 1, 1994.